Materials Today Energy 12 (2019) 129–135

Contents lists available at ScienceDirect

Materials Today Energy

journal homepage: www.journals.elsevier.com/materials-today-energy/

Incorporation of gold nanocages into electrospun nanofibers for efficient water evaporation through photothermal heating

Tong Wu [a, b], Haoxuan Li [a], Minghao Xie [c], Song Shen [a], Wenxia Wang [a], Ming Zhao [c], Xiumei Mo [b], Younan Xia [a, c, d, *, 1]

[a] The Wallace H. Coulter Department of Biomedical Engineering, Georgia Institute of Technology and Emory University, Atlanta, GA 30332, USA
[b] State Key Lab for Modification of Chemical Fibers and Polymer Materials, College of Chemistry, Chemical Engineering and Biotechnology, Donghua University, Shanghai 201620, PR China
[c] School of Chemistry and Biochemistry, Georgia Institute of Technology, Atlanta, GA 30332, USA
[d] School of Chemical and Biomolecular Engineering, Georgia Institute of Technology, Atlanta, GA 30332, USA

ARTICLE INFO

Article history:
Received 12 December 2018
Accepted 20 December 2018

Keywords:
Electrospun nanofiber
Gold nanocage
poly(vinylidene fluoride)
Nonwoven mat
Water evaporation

ABSTRACT

Conventional techniques for water desalination and purification are relatively low in efficiency because they typically involve the placement of a heating unit at the bottom of the container to boil the entire liquid volume. Herein we report the incorporation of Au nanocages (AuNCs) into electrospun nanofibers of poly(vinylidene fluoride) (PVDF) for efficient water evaporation *via* photothermal heating. Because PVDF is highly hydrophobic, its nonwoven mat naturally floats on the surface of water. Upon irradiation with a near-infrared (NIR) laser at 808 nm, the water at the surface is heated to evaporate while the bulk remains at the ambient temperature. As such, the efficiency for water evaporation is greatly increased. To further demonstrate the potential of AuNC/PVDF nanofiber mats for solar water evaporation, we prepare AuNCs with a broad absorption peak covering the visible and NIR regions. Under natural solar irradiation (1000 W m^{-2}), water evaporation efficiencies as high as 67.0% and 79.8% are achieved when using the AuNC/PVDF nanofiber mats containing AuNCs at weight percentages of 0.05% and 0.10%, respectively. The performance is comparable or even greater than most of the reported floating devices under the illumination of sun concentration systems. This new system paves the way to the design and fabrication of sustainable and scalable floating membranes for water desalination and purification.

1. Introduction

Efficient conversion from solar energy to heat for the generation of water vapor or steam is vital to an array of applications, especially for desalination and purification to produce pure water [1,2]. Conventional techniques for solar steam generation often involve the use of costly and heavy optical concentration systems to boil the entire volume of a water source [3,4]. Because of the transfer of energy to the non-evaporative portion of water in the bulk, there is inevitable waste of heat or energy. As a result, these techniques are not ideal for large-scale operation. Although a variety of highly absorbing materials such as charcoal [5], sponge [6], or cotton cloth [7] have been utilized to enhance solar absorption, the efficiency of energy conversion is still relatively low, typically around 30–45% [8].

Water evaporation is a surface process, in which only the molecules at the air-water interface are transformed into the vapor phase upon the input of adequate energy [4]. In this regard, floating devices such as those based upon carbon foam [9], wood [10], mushroom [11], paper [1,12], gel [13,14], and various types of plasmon-enhanced substrates [15–22] have been explored to localize the absorbing material at the surface of a water source to improve the evaporation efficiency. To this end, it is necessary to ensure self-floating capability with surface hydrophobicity so that the light-absorbing material can be retained at the air-water interface, enabling continuous solar heating and thus water evaporation at the interface [4].

There is a major incentive in using electrospun nanofibers with plasmonic heating capability for water evaporation [23]. Because of their intrinsic high porosity, interconnectivity, and surface-to-

* Corresponding author. The Wallace H. Coulter Department of Biomedical Engineering, Georgia Institute of Technology and Emory University, Atlanta, GA 30332, USA.
E-mail address: younan.xia@bme.gatech.edu (Y. Xia).
[1] Lead Contact.

https://doi.org/10.1016/j.mtener.2018.12.008
2468-6069/

volume ratio, nonwoven mats comprised of electrospun nanofibers are excellent candidates for water evaporation [24]. Herein, we demonstrate the incorporation of plasmonic nanostructures into electrospun nanofibers to harvest photon energy as an effective means for water evaporation without the use of costly solar concentrating systems. We chose to focus on PVDF as a membrane material owing to its electrospinning capability and many other attractive properties such as hydrophobicity, flexibility, low toxicity, and a high melting point [25]. Besides, PVDF is relatively inexpensive and can be easily processed [26]. The electrospun nanofiber mats comprised of PVDF also show promising prospects in terms of large-scale production and recyclability [27]. As a major advantage over many other polymers, PVDF has piezoelectric and pyroelectric activities [25], which can be potentially utilized for synchronized water evaporation and electricity generation.

Gold nanoparticles represent a typical class of plasmonic nanostructures used for photothermal applications. For the conventional Au nanoparticles with a solid interior and quasi-spherical shape, their localized surface plasmon resonance (LSPR) peaks are typically limited to the visible region [28]. Only those with anisotropic (*e.g.*, rods, multipods, and stars) or hollow structures (*e.g.*, shells, boxes, and cages) can display LSPR peaks tunable in the entire visible and NIR regions [29]. Among the later class of Au nanostructures, Au nanocages (AuNCs) with hollow interiors and porous walls are particularly advantageous because of their hollow interiors in saving the material and cutting the cost. In addition, the LSPR of AuNCs is typically dominated by absorption rather than scattering while the peak position can be precisely tuned to any wavelength of interest in the range of 400–1200 nm by controlling the wall thickness and porosity of the walls [29–32].

In a typical study, we prepare AuNCs with an LSPR peak around 800 nm and directly disperse them in a PVDF solution for electrospinning to obtain AuNC/PVDF nanofiber mats. When floating on water, the AuNCs in the nanofiber mat generate heat upon irradiation by a NIR laser, leading to highly efficient light-to-heat conversion. The terminal temperature and heating time can be adjusted by changing the weight percentage of AuNCs in PVDF and/or the light intensity, allowing for the fabrication of AuNC/PVDF mats with optimal performance in terms of cost and terminal temperature. We also prepare a mixture of AuNCs with a broad absorption peak covering the visible and NIR regions and incorporate them into PVDF nanofibers. The resultant nanofiber mats show great potential in utilizing the maximum energy of solar irradiation for water evaporation.

2. Results and discussion

2.1. Surface hydrophobicity of the PVDF electrospun nanofibers and its significance

We first evaluated the importance of PVDF's hydrophobicity in keeping a mat of its nanofibers at the air-water interface. Fig. S1 shows the photographs of a PVDF nanofiber mat, a plasma-treated PVDF nanofiber mat, and a nanofiber mat made of a blend of PCL and gelatin at a weight ratio of 1:1, respectively, when the samples were placed in water. Since PVDF is hydrophobic, its nanofiber mat was able to naturally float on the water surface and maintain its position at the air-water interface. After treating both sides of a PVDF nanofiber mat with oxygen plasma to make the surface hydrophilic, the mat was submerged in water. In contrast, the hydrophilic nanofiber mat made of a blend of PCL and gelatin sank to the bottom of water. This simple demonstration illustrates the critical importance to use a hydrophobic polymer such as PVDF to ensure that the AuNC-loaded nanofiber mat will float at the air-water interface during the entire process of water evaporation.

2.2. Characterizations of AuNCs and AuNC/PVDF electrospun nanofibers

A prior study reported that Au nanoshells could be fabricated with tunable absorption and minimized scattering, yielding a higher solar vapor generation rate relative to their counterparts with a solid core [33]. Similarly, the LSPR peaks of AuNCs can also be readily tuned to cover the entire visible and NIR regions. However, the absorption cross-sections of AuNCs are more than two times greater than that of Au nanoshells [28]. As such, AuNCs represent a better transducer for more effective photothermal conversion.

Our initial focus was placed on the AuNCs with an LSPR peak located at 786 nm, as shown by the UV–vis–NIR absorption spectrum in Fig. 1A. The inset shows a transmission electron microscopy (TEM) image of the AuNCs, which had a well-defined hollow interior, together with an outer edge length of about 50.7 nm and a wall thickness of roughly 5.8 nm. According to inductively-coupled plasma mass spectrometry (ICP-MS) data, the AuNCs had an elemental composition of $Au_{52}Ag_{48}$. We also recorded UV–vis–NIR absorption spectra from an aqueous suspension of AuNC/PVDF nanofibers (Fig. 1A). Upon loading into PVDF nanofibers, the LSPR peak of the AuNCs was red-shifted from 786 nm to 813 nm due to the change in surrounding environment from water to PVDF. This red-shift would allow for a good overlap with the output of a diode laser peaked at 808 nm and thus maximization of the photothermal heating effect. For the suspension of AuNC/PVDF nanofibers, the strong extinction of light in the range of 300–600 nm can be attributed to the scattering of light by the scattering of nanofibers [34], as confirmed by the UV–vis–NIR spectra in Fig. S2 recorded from an aqueous suspension of PVDF nanofibers and a thin film of PVDF, respectively. As expected, light scattering was greatly enhanced when moving from cast films to nonwoven mats of nanofibers due to the small lateral dimensions of the nanofibers. Fig. S3 shows the UV–vis–NIR spectra of another set of AuNCs and AuNC/PVDF nanofibers (both as aqueous suspensions) up to nearly 1400 nm, allowing for clear resolution of the LSPR peak positions.

Fig. 1B shows photographs of the as-obtained AuNC/PVDF and PVDF nanofiber mats. Different from the white color of the PVDF nanofiber mat, the AuNC/PVDF nanofiber mat showed a light blue tint, resembling the color displayed by the aqueous suspension of AuNCs. Fig. 1C and D, shows scanning electron microscopy (SEM) images of the AuNC/PVDF and PVDF nanofibers, respectively. The average diameter of the AuNC/PVDF nanofibers was 280.63 ± 41.45 nm, compared with 304.85 ± 37.74 nm for the PVDF nanofibers. To verify the incorporation of AuNCs into PVDF nanofibers, we recorded and compared the UV–vis–NIR absorption spectra recorded from the AuNC/PVDF and PVDF nanofiber mats after the mats had been dissolved in N,N-Dimethylformamide (DMF). As shown in Fig. S4, there was an absorption peak around 800 nm for the sample derived from the AuNC/PVDF nanofiber mat, whereas no absorption peak was observed in the case of PVDF nanofiber mat. We then characterized one individual AuNC/PVDF nanofiber by TEM. The image in Fig. S5 clearly demonstrated the presence of AuNCs inside the PVDF nanofiber.

2.3. Temperature increase for AuNC/PVDF nanofiber mat under NIR irradiation

In one study, we characterized the NIR-induced heating in a AuNC/PVDF nanofiber mat containing AuNCs at a weight percentage of 0.05%. We used a diode laser with an output peaked at 808 nm to allow for a good overlap with the LSPR peak (around 813 nm) of the mat and thus maximization of the photothermal heating effect. Upon exposure to the NIR laser, we monitored the

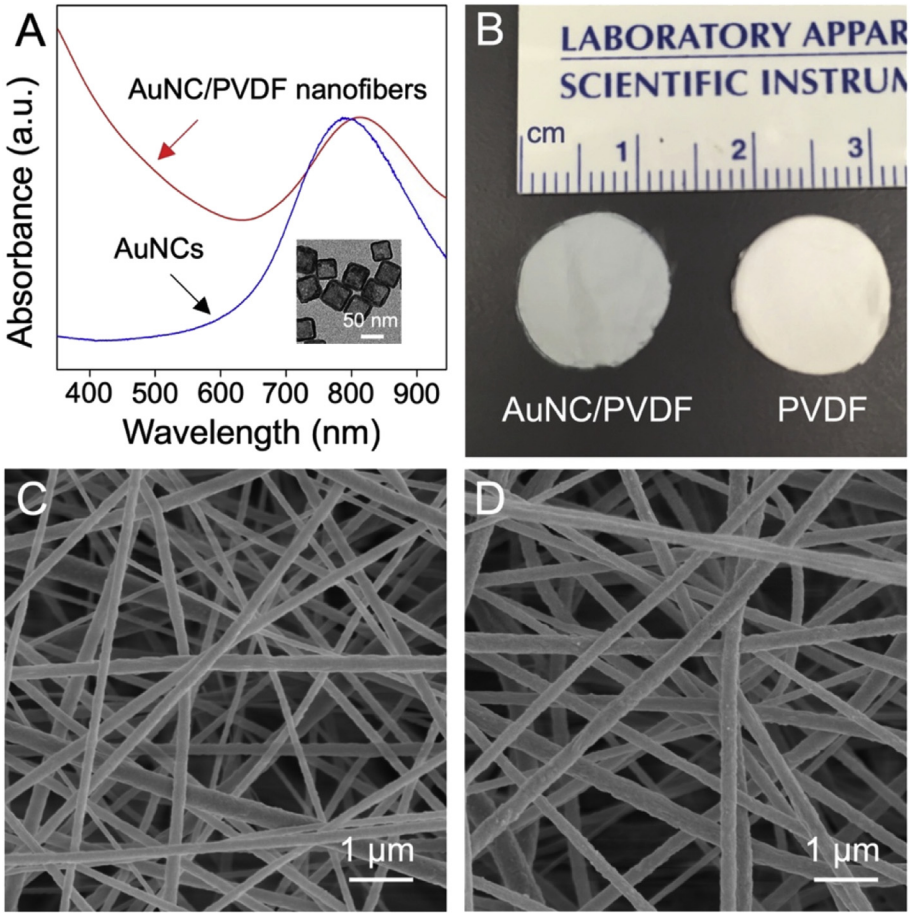

Fig. 1. Characterizations of AuNCs and electrospun nanofibers made of AuNC/PVDF and PVDF, respectively. (A) UV–vis–NIR extinction spectra recorded from aqueous suspensions of AuNCs (blue line) and AuNC/PVDF nanofibers (red line). The inset shows a typical TEM image of the AuNCs. It should be pointed out that the spectra were normalized to their peak intensity around 800 nm, respectively. The exact absorbance values of these two samples cannot be directly compared as different amounts of materials might be involved for the measurements. (B) Photographs and (C, D) SEM images of (C) AuNC/PVDF and (D) PVDF nanofiber mats, respectively.

temperatures of the AuNC/PVDF nanofiber mat using a K-type thermocouple and an infrared (IR) camera (see Supplemental Experimental Procedures). The images in Fig. 2A show the surface temperatures of the AuNC/PVDF and PVDF nanofiber mats placed in air before and after laser irradiation. Fig. S6A shows the corresponding photographs of the PVDF and AuNC/PVDF nanofiber mats before and after NIR laser irradiation. The PVDF nanofiber mat showed essentially no change in temperature upon laser irradiation. In comparison, the surface temperature of the AuNC/PVDF nanofiber mat reached 120.0 °C only after irradiation with the laser at a power density of 0.4 W cm^{-2} for 30 s. The increase in temperature is mainly caused by the photothermal heating effect of the AuNCs and the poor thermal conductivity of the air surrounding the nanofibers. Fig. 2B shows the temperatures of the AuNC/PVDF nanofiber mat when it was irradiated with the NIR laser for 4 min at different power densities. The photothermal heating effect resulted in temperature increases to 81.4 and 136.0 °C upon irradiation at power densities of 0.2 and 0.4 W cm^{-2}, respectively. When the power density was further increased to 0.8 W cm^{-2}, the surface temperature of the AuNC/PVDF mat quickly rose to 150 °C in 30 s. In this case, the mat started to melt because the temperature was close to the melting point (around 170 °C) of PVDF. As such, we chose a power density of 0.4 W cm^{-2} for all the demonstrations. Compared with the drastic increase in temperature observed for the AuNC/PVDF nanofiber mat, the PVDF nanofiber mat showed almost no change in temperature during NIR irradiation under the same condition (Fig. 2C).

We also carried out the same measurements for the AuNC/PVDF nanofiber mats containing AuNCs at different weight percentages of 0.01%, 0.02%, and 0.10%, respectively (see Supplemental Experimental Procedures). As shown in Fig. S7, all the AuNC/PVDF mats showed drastic increases in temperature upon NIR irradiation relative to the case of a PVDF nanofiber mat. As expected, the maximum temperature recorded for the AuNC/PVDF mat increased as the weight percentage of AuNCs was increased.

2.4. Water evaporation by heating the AuNC/PVDF nanofiber mat with NIR irradiation

In demonstrating its potential use in water evaporation, we firstly measured the surface temperature of AuNC/PVDF and PVDF nanofiber mats when they were floating on water and irradiated by the NIR laser at a power density of 0.4 W cm^{-2}, see the IR images in Fig. 3A. Fig. S6B shows the corresponding photographs of the PVDF and AuNC/PVDF nanofiber mats before and after NIR laser irradiation. Within 15 min, the temperature of the interface between the AuNC/PVDF mat and air was increased to 96 °C, while the interface remained at 28 °C in the case of PVDF nanofiber mat. It is clear that photothermal heating was induced by the AuNCs upon laser irradiation [12,21], contributing to a much greater temperature in the

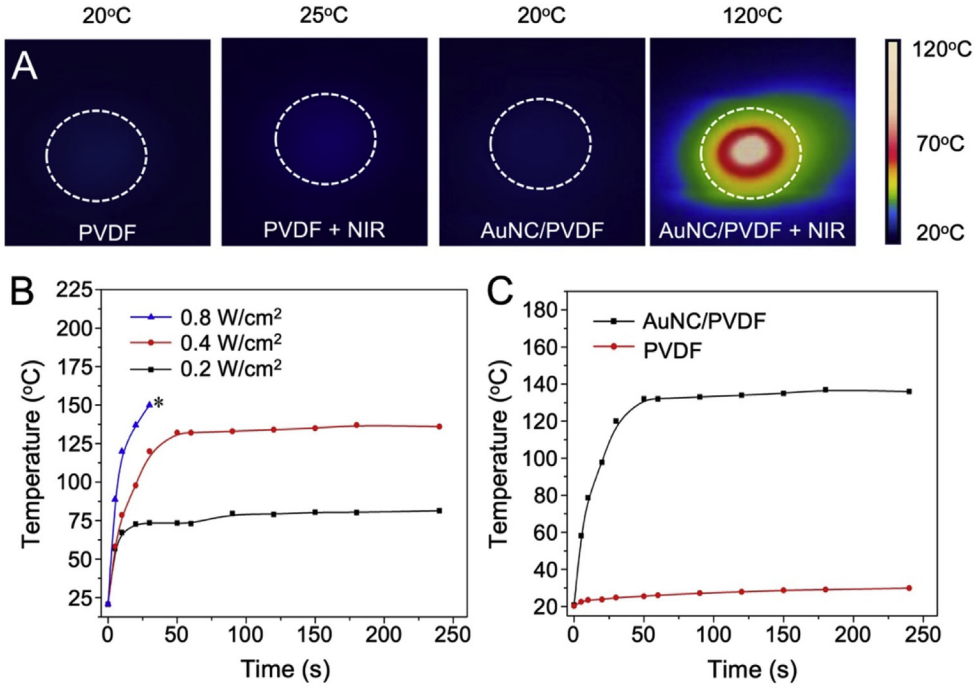

Fig. 2. Temperature increase in the AuNC/PVDF and PVDF nanofiber mats placed in air upon NIR laser irradiation. (A) Surface temperatures (measured using an IR camera) of AuNC/PVDF and PVDF nanofiber mats before and after NIR irradiation with the laser at a power density of 0.4 W cm^{-2} for 30 s. The circle marked by dashed lines indicates the location of the nanofiber mat. (B) Temperatures (measured using a thermo-couple) of the AuNC/PVDF nanofiber mat during 4 min of laser irradiation at power densities of 0.2, 0.4, and 0.8 W cm^{-2}, respectively. *indicates the temperature was higher than 150 °C so the mat started to melt. (C) Comparison of the AuNC/PVDF and PVDF nanofiber mats in terms of temperature after 4 min of irradiation with the laser at a power density of 0.4 W cm^{-2}.

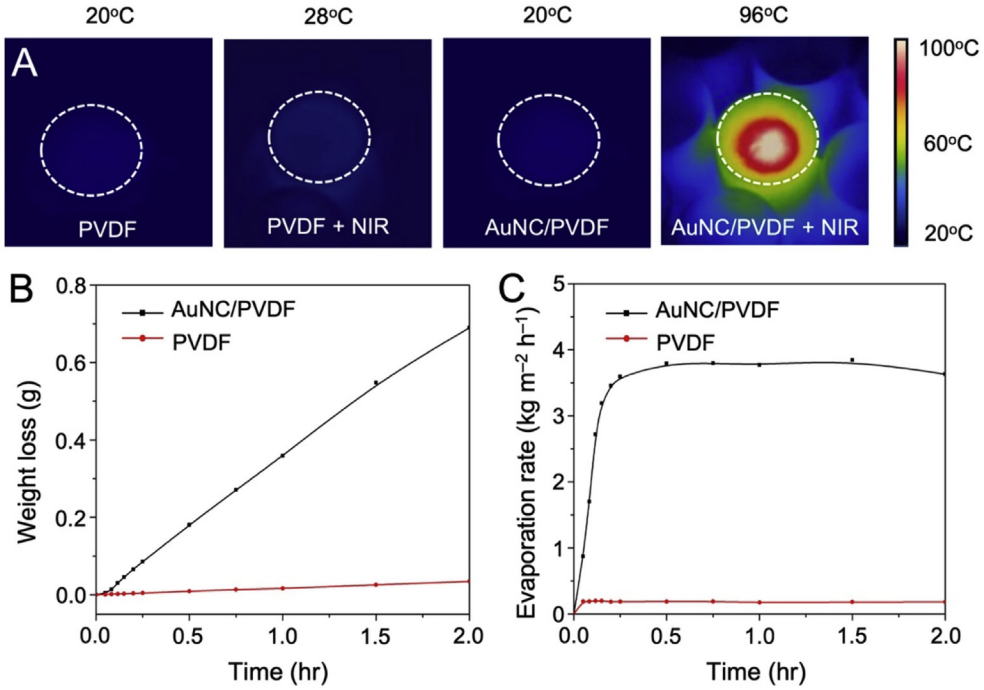

Fig. 3. Water evaporation by heating the AuNC/PVDF and PVDF nanofiber mats with NIR irradiation. (A) Surface temperatures of AuNC/PVDF and PVDF nanofiber mats when they were floating on water before and after NIR laser irradiation at a power density of 0.4 W cm^{-2} for 15 min. The circle marked by dashed lines indicates the location of the nanofiber mat. (B) Weight loss of water as a function of time when AuNC/PVDF and PVDF nanofiber mats were floating on water and irradiated by the laser at power density of 0.4 W cm^{-2} over a period of 2 h, respectively. (C) Water evaporation rate as a function of time when AuNC/PVDF and PVDF nanofiber mats were floating on water and irradiated by the laser at a power density of 0.4 W cm^{-2} over a period of 2 h, respectively.

AuNC/PVDF mat relative to the PVDF counterpart. We also compared the temperature increase profiles for the AuNC/PVDF nanofiber mats when they were placed in air or floating on water surface (the pristine mat), submerged in water (after plasma treatment), and fixed to the bottom of the container (using a biomedical glue), respectively, upon irradiation with the laser at a power density of 0.4 W cm^{-2} over a period of 240 s (in air) or 1200 s (in water). The results confirmed that the temperature was not able to reach 60 °C when the mat was submerged in water or fixed to the bottom of the container (Fig. S8), simply because water is a much better thermal conductor than air to allow for much quicker heat dissipation.

We then examined the water evaporation performance of the AuNC/PVDF nanofiber mat in comparison to the pristine PVDF nanofiber mat upon NIR irradiation at a power density of 0.4 W cm^{-2}. The weight loss of water is plotted as a function of time over a period of 2 h in Fig. 3B. The loss of water due to evaporation was 0.69 ± 0.02 g in the presence of AuNC/PVDF nanofiber mat on the top surface, whereas almost no weight loss was recorded in the case of PVDF nanofiber mat. Under the mediation of AuNC/PVDF nanofiber mat, the rate of water evaporation gradually increased to 3.64 ± 0.06 kg m^{-1} h^{-1} in 15 min upon laser irradiation and then remained stable until the measurement was stopped (Fig. 3C). In this case, the AuNC/PVDF nanofiber mat could serve as a thermal insulating layer to reduce the heat transfer between the vaporization region (the water surface) and the bulk liquid [1]. Because of the capillary action associated with the fibrous structure, localized water evaporation was realized throughout the nanofiber mat. In comparison, the rate of water evaporation was negligible when a PVDF nanofiber mat was used under the same condition.

To demonstrate the feasibility to reuse the AuNC/PVDF nanofibers, we applied the same mat to 10 rounds of measurement and then derived the water evaporation rates at different rounds under the same condition. For each round, the AuNC/PVDF nanofiber mat on the water surface was irradiated by the NIR laser at a power density of 0.4 W cm^{-2}. After operation for 2 h, the wet AuNC/PVDF mat was completely dried in an oven before applying to the next round. Fig. 4A compares the water evaporation rates obtained in different rounds of measurement. The water evaporation rate was stable in the range of 3.40–3.57 kg m^{-2} h^{-1}, demonstrating excellent stability of the AuNC/PVDF nanofiber mat. Note that the evaporation rates were plotted after subtracting the background data obtained from measurements in the dark environment (0.18 kg m^{-2} h^{-1}). The rates were subsequently used to calculate the conversion efficiency. Considering the relatively low cost, high hydrophobicity, good thermal/chemical stability, and high mechanical strength associated with PVDF [35,36], the AuNC/PVDF nanofiber mats are particularly attractive for long-term and large-scale water evaporation. We calculated the light-to-heat conversion efficiency (η), known as the evaporation efficiency, of the AuNC/PVDF nanofiber mat as a function of round of operation according to a previously reported method (see Supplemental Experimental Procedures) [9,12]. As shown in Fig. 4B, the average conversion efficiency of the mat was 60.9% under the NIR laser irradiation at a power density of 0.4 W cm^{-2}. During the 10 rounds of operation, the mat showed stable performance, with an almost constant conversion efficiency in the range of 59.3–63.5%. This conversion efficiency is higher than what was achieved using the conventional solar vapor generation system, where the light absorbing material was usually placed at the bottom of the basin to heat the entire liquid volume with a fairly low efficiency in the range of 30–45% [4,37]. Also, the conversion efficiency of the AuNC/PVDF nanofiber mat under NIR laser irradiation was greater than what was reported for a system that directly dispersed Au nanoparticles in water for solar vapor generation (24%) [38].

To demonstrate the potential of the AuNC/PVDF nanofiber mats in seawater desalination and waste water purification, the as-prepared mats were floating on the surface of an aqueous NaCl or dye solution. The weight loss and hourly output of water were 1.55 ± 0.04 g and 2.68 ± 0.04 L m^{-2} h^{-1}, respectively, in the case of NaCl solution upon laser irradiation at a power density of 0.4 W cm^{-2} over a period of 5 h (Fig. 4C). As shown in Fig. 4D, the weight loss and hourly output of water were 1.45 ± 0.04 g and 2.94 ± 0.04 L m^{-2} h^{-1}, respectively, in the case of dye solution. We also confirmed that clean water could be collected in both cases, showing the potential of the AuNC/PVDF nanofiber mats for applications related to water desalination and purification.

2.5. Water evaporation by heating the AuNC/PVDF nanofiber mat with solar irradiation

Evaporation driven by solar energy has been widely utilized in commercial applications [39,40]. To further demonstrate the potential of the AuNC/PVDF nanofiber mats for solar water evaporation, we prepared a sample of AuNCs with a very broad absorption peak covering the visible and NIR regions from 500 to 1000 nm (see Supplemental Experimental Procedures and Figs. S9–S10). We then prepared disks of the AuNC/PVDF nanofiber mats (4 cm in diameter) containing AuNCs at different weight percentages of 0.05% and 0.10%, respectively. The nanofiber mat made of PVDF nanofibers was also tested for comparison. The weight loss of water was recorded with the nanofiber mat floating on water upon solar irradiation over a period of 8 h in the outdoor environment with an air temperature around 25 °C in Atlanta. At 8 h post solar irradiation, the weight losses of water in the cases of AuNC/PVDF mats were 10.73 g (for 0.05% of AuNCs) and 12.78 g (for 0.10% of AuNCs), respectively, relative to 3.02 g for the mat made of pure PVDF (Fig. S11A). The water evaporation rates were 1.07 kg m^{-2} h^{-1} (for 0.05% of AuNCs) and 1.27 kg m^{-2} h^{-1} (for 0.10% of AuNCs), respectively, in the cases of AuNC/PVDF mats, which represent 3.57- and 4.23-fold, respectively, increase relative to that (0.30 kg m^{-2} h^{-1}) of a mat made of pure PVDF (Fig. S11B). The slight evaporation of water in the case of PVDF mat can be attributed to natural water evaporation. We also applied the AuNC/PVDF mat to 10 rounds of measurement at a similar temperature on sunny days in Atlanta, and Fig. S12 show photographs of the AuNC/PVDF and PVDF nanofiber mats after 10 rounds of measurement. The water evaporation rates at different rounds remained stable in the range of 1.03–1.12 kg m^{-2} h^{-1} (for 0.05% of AuNCs) and 1.21–1.30 kg m^{-2} h^{-1} (for 0.10% of AuNCs), respectively, after solar irradiation for 8 h.

We then estimated the water evaporation efficiencies when using the AuNC/PVDF nanofiber mats under normal solar illumination (1000 W m^{-2}) (see Supplemental Experimental Procedures) [11]. The evaporation efficiencies reached 67.0% and 79.8% for the AuNC/PVDF nanofiber mats containing AuNCs at weight percentages of 0.05% and 0.10%, respectively. Note that the water evaporation efficiencies also included the contribution from natural water evaporation as we performed the experiments under natural sunlight. As such, we used PVDF nanofiber mat free of AuNCs as a control. Compared with the low evaporation efficiency (18.9%) of pure PVDF nanofiber mat that was attributed to the natural water evaporation, the broadband absorption peak of the AuNCs in the visible and NIR regions contributed significantly to the highly efficient energy conversion from solar energy to heat.

Table S1 shows a comparison of solar water evaporation performance based on photothermal heating with plasmonic nanostructures or other types of materials. At a low weight percentage of 0.05 or 0.10% for the AuNCs, the performance of the AuNC/PVDF nanofiber mats under normal solar illumination was comparable and even greater than that of the reported floating membranes

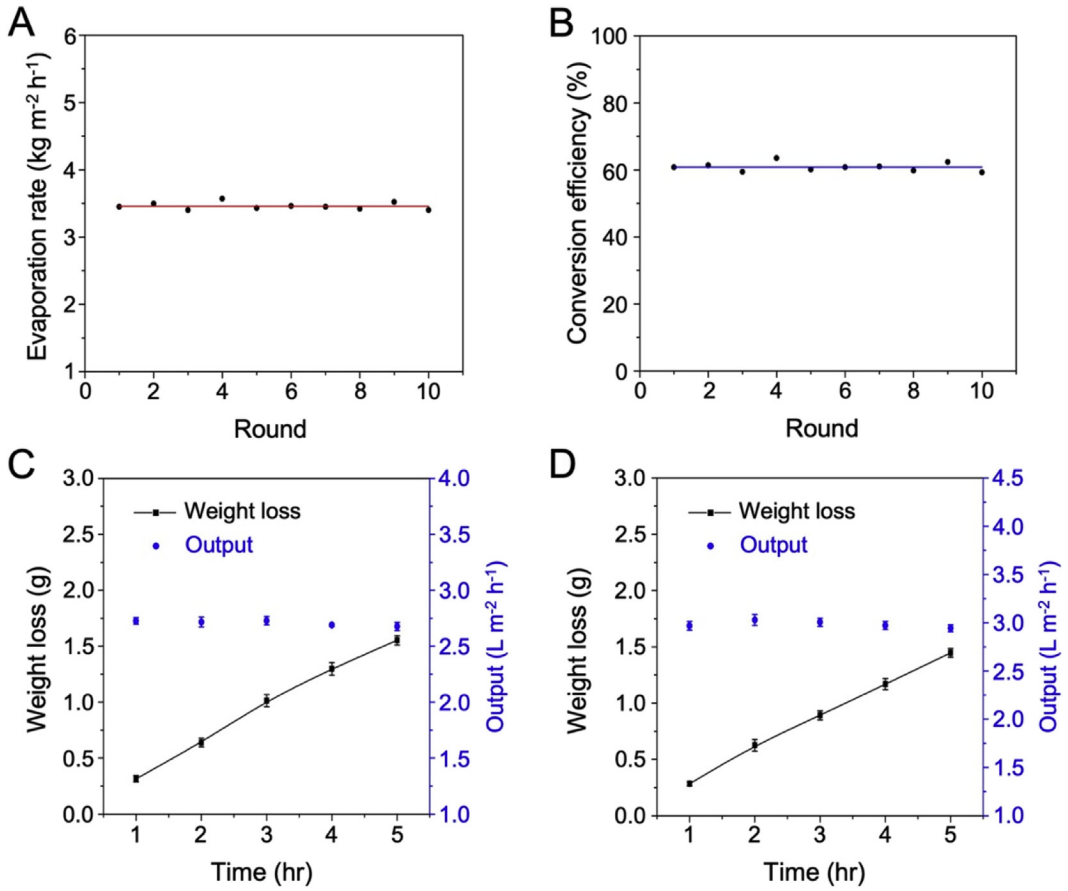

Fig. 4. Recyclability of the AuNC/PVDF nanofiber mat for water evaporation and a proof-of-concept demonstration for water desalination and purification. (A) Water evaporation rates during the 10 rounds of measurements with the AuNC/PVDF nanofiber mat floating on water and irradiated by the laser at a power density of 0.4 W cm^{-2} for 2 h. Note that the evaporation rates were plotted after subtracting the background data obtained from measurements in the dark environment (0.18 kg m^{-2} h^{-1}). The rates were subsequently used to calculate the conversion efficiency in (B). (B) Light-to-heat conversion efficiency during the 10 rounds of measurement with the AuNC/PVDF nanofiber mat floating on water and irradiated by the laser at a power density of 0.4 W cm^{-2} for 2 h. The straight lines in (A) and (B) are linear fitting to the data points, respectively, corresponding to the average values of water evaporation rate and light-to-heat conversion efficiency. Aqueous solutions containing (C) NaCl and (D) dye, respectively, were separately utilized for proof-of-concept demonstrations of water desalination and purification. The weight loss and hourly output of water were measured, respectively, with the AuNC/PVDF nanofiber mat floating on the aqueous NaCl or dye solution and irradiated by the laser at a power density of 0.4 W cm^{-2} over a period of 5 h.

operated under the illumination of sun concentration systems, including the black Au membranes (57% under 20 Sun solar irradiation) [15], air-laid-papers with Au nanoparticles (77.8% under 4.5 Sun solar irradiation) [12], carbon nanotube-modified wood membranes (65%, 67%, 72%, and 77% under solar irradiation at 1, 3, 5, and 7 Sun, respectively) [41], black TiO_x ($x < 2$) coated-stainless steel mesh (50.3% under 1 Sun solar irradiation) [42], and aerogels made of cellulose nanofibrils and carbon nanotubes (76.3% under 1 Sun solar irradiation) [13]. In comparation to the solar steam generation devices used in these studies, the AuNC/PVDF nanofiber mats show immediate advantages such as high energy conversion efficiency, tunable weight percentage of AuNCs, reusability, and unnecessity of using costly solar concentrating systems. In terms of scaling up the AuNC/PVDF nanofiber mats for large-scale water evaporation, needleless electrospinning can be used to fabricate the nanofiber mats on an industrial scale [27]. To meet the cost requirements, we can optimize the weight percentage of AuNCs in PVDF and the morphology of nanofibers to obtain AuNC/PVDF nanofiber mats with a practical evaporation efficiency for freshwater production.

3. Conclusion

We have demonstrated the incorporation of AuNCs into electrospun PVDF nanofibers to locally heat the interfacial water for the purpose of efficient water evaporation. The plasmon-assisted conversion from light to heat is realized at the water-air interface owing to the high hydrophobicity of PVDF and the photothermal heating effect of AuNCs. This new system is well-suited for water evaporation, with a considerably greater evaporation efficiency relative to the conventional bulk heating systems. In comparison to most of the reported floating devices, the AuNC/PVDF nanofiber mats show comparable and even better solar-to-heat conversion efficiencies. By integrating the remarkable photothermal effect of AuNCs with low-cost and hydrophobic PVDF nanofibers, we provide a new route to fabricate reusable and scalable floating mats with optimal conversion efficiencies for water evaporation without the use of costly solar concentrating systems. We believe this work extends the flexibility of electrospun nanofiber mats in environmental engineering and forecasts a new system of efficient solar heating to address world water and energy issues.

4. Experimental procedures

Fabrication and characterization of AuNCs and AuNC/PVDF nanofibers, water evaporation measurements under near-infrared and solar irradiations are provided in the Supplemental Experimental Procedures.

Author contributions

Y.X. conceived the idea and designed the experiments. Y.X. and X.M. directed the project. T.W. carried out the experiments. H.L. assisted T.W. in preparing the Au nanocages. M.X. performed the discrete dipole approximation (DDA) calculation. S.S. and W.W. performed the TEM characterization. M.Z. performed the ICP-MS characterization. Y.X. and T.W. wrote and revised the manuscript.

Declaration of interests

The authors declare no conflict of interest.

Acknowledgments

This work was supported by startup funds from the Georgia Institute of Technology. As jointly supervised Ph.D. candidates from Donghua University, T.W. and H.L. were also partially supported by fellowships from the China Scholarship Council.

Appendix A. Supplementary data

Supplementary data to this article can be found online at https://doi.org/10.1016/j.mtener.2018.12.008.

References

[1] Z. Liu, H. Song, D. Ji, C. Li, A. Cheney, Y. Liu, N. Zhang, X. Zeng, B. Chen, J. Gao, et al., Extremely cost-effective and efficient solar vapor generation under non-concentrated illumination using thermally isolated black paper, Global Chall. 1 (2017) 1600003.
[2] G.M. Ayoub, L. Malaeb, Developments in solar still desalination systems: a critical review, Crit. Rev. Environ. Sci. Technol. 42 (2012) 2078–2112.
[3] A. Lenert, E.N. Wang, Optimization of nanofluid volumetric receivers for solar thermal energy conversion, Sol. Energy 86 (2012) 253–265.
[4] L. Zhang, B. Tang, J. Wu, R. Li, P. Wang, Hydrophobic light-to-heat conversion membranes with self-healing ability for interfacial solar heating, Adv. Mater. 27 (2015) 4889–4894.
[5] M.M. Naim, M.A.A. El Kawi, Non-conventional solar stills part 1. non-conventional solar stills with charcoal particles as absorber medium, Desalination 153 (2003) 55–64.
[6] B.A. Abu-Hijleh, H.M. Rababa'h, Experimental study of a solar still with sponge cubes in basin, Energy Convers. Manag. 44 (2003) 1411–1418.
[7] K.K. Murugavel, K. Srithar, Performance study on basin type double slope solar still with different wick materials and minimum mass of water, Renew. Energy 36 (2011) 612–620.
[8] P. Durkaieswaran, K.K. Murugavel, Various special designs of single basin passive solar still–a review, Renew. Sustain. Energy Rev. 49 (2015) 1048–1060.
[9] H. Ghasemi, G. Ni, A.M. Marconnet, J. Loomis, S. Yerci, N. Miljkovic, G. Chen, Solar steam generation by heat localization, Nat. Commun. 5 (2014) ncomms5449.
[10] K.K. Liu, Q. Jiang, S. Tadepalli, R. Raliya, P. Biswas, R.R. Naik, S. Singamaneni, Wood-graphene oxide composite for highly efficient solar steam generation and desalination, ACS Appl. Mater. Interfaces 9 (2017) 7675–7681.
[11] N. Xu, X. Hu, W. Xu, X. Li, L. Zhou, S. Zhu, J. Zhu, Mushrooms as efficient solar steam-generation devices, Adv. Mater. 29 (2017) 1606762.
[12] Y. Liu, S. Yu, R. Feng, A. Bernard, Y. Liu, Y. Zhang, H. Duan, W. Shang, P. Tao, C. Song, T. Deng, A bioinspired, reusable, paper-based system for high-performance large-scale evaporation, Adv. Mater. 27 (2015) 2768–2774.
[13] F. Jiang, H. Liu, Y. Li, Y. Kuang, X. Xu, C. Chen, H. Huang, C. Jia, X. Zhao, E. Hitz, et al., Lightweight, mesoporous, and highly absorptive all-nanofiber aerogel for efficient solar steam generation, ACS Appl. Mater. Interfaces 10 (2017) 1104–1112.
[14] F. Zhao, X. Zhou, Y. Shi, X. Qian, M. Alexander, X. Zhao, S. Mendez, R. Yang, L. Qu, G. Yu, Highly efficient solar vapour generation via hierarchically nanostructured gels, Nat. Nanotechnol. 13 (2018) 489–495.
[15] K. Bae, G. Kang, S.K. Cho, W. Park, K. Kim, W.J. Padilla, Flexible thin-film black gold membranes with ultrabroadband plasmonic nanofocusing for efficient solar vapour generation, Nat. Commun. 6 (2015) 10103.
[16] L. Zhou, Y. Tan, D. Ji, B. Zhu, P. Zhang, J. Xu, Q. Gan, Z. Yu, J. Zhu, Self-assembly of highly efficient, broadband plasmonic absorbers for solar steam generation, Sci. Adv. 2 (2016) e1501227.
[17] L. Zhou, Y. Tan, J. Wang, W. Xu, Y. Yuan, W. Cai, S. Zhu, J. Zhu, 3D self-assembly of aluminium nanoparticles for plasmon-enhanced solar desalination, Nat. Photon. 10 (2016) 393–398.
[18] L. Zhou, S. Zhuang, C. He, Y. Tan, Z. Wang, J. Zhu, Self-assembled spectrum selective plasmonic absorbers with tunable bandwidth for solar energy conversion, Nano Energy 32 (2017) 195–200.
[19] C. Liu, J. Huang, C.E. Hsiung, Y. Tian, J. Wang, Y. Han, A. Fratalocchi, High-performance large-scale solar steam generation with nanolayers of reusable biomimetic nanoparticles, Adv. Sustainable Syst. 1 (2017) 1600013.
[20] M. Kaur, S. Ishii, S.L. Shinde, T. Nagao, All-ceramic microfibrous solar steam generator: tin plasmonic nanoparticle-loaded transparent microfibers, ACS Sustain. Chem. Eng. 5 (2017) 8523–8528.
[21] L. Yi, S. Ci, S. Luo, P. Shao, Y. Hou, Z. Wen, Scalable and low-cost synthesis of black amorphous Al-Ti-O nanostructure for high-efficient photothermal desalination, Nano Energy 41 (2017) 600–608.
[22] F. Tao, Y. Zhang, K. Yin, S. Cao, X. Chang, Y. Lei, D.S. Wang, R. Fan, L. Dong, Y. Yin, et al., Copper sulfide-based plasmonic photothermal membrane for high-efficiency solar vapor generation, ACS Appl. Mater. Interfaces 10 (2018) 35154–35163.
[23] M. Chen, Y. Wu, W. Song, Y. Mo, X. Lin, Q. He, B. Guo, Plasmonic nanoparticle-embedded poly(p-phenylene benzobisoxazole) nanofibrous composite films for solar steam generation, Nanoscale 10 (2018) 6186–6193.
[24] S. Ramakrishna, K. Fujihara, W.E. Teo, T. Yong, Z. Ma, R. Ramaseshan, Electrospun nanofibers: solving global issues, Mater. Today 9 (2006) 40–50.
[25] H. Li, T. Wu, M. Xie, Y. Shi, S. Shen, M. Zhao, X. Yang, L. Figueroa-Cosme, Q. Ke, Y. Xia, Enhancing the tactile and near-infrared sensing capabilities of electrospun PVDF nanofibers with the use of gold nanocages, J. Mater. Chem. C 6 (2018) 10263–10269.
[26] G. Mader, H. Meixner, Pyroelectric infrared sensor arrays based on the polymer PVDF, Sens. Actuators, A 22 (1990) 503–507.
[27] J. Fang, H. Niu, H. Wang, X. Wang, T. Lin, Enhanced mechanical energy harvesting using needleless electrospun poly(vinylidene fluoride) nanofibre webs, Energy Environ. Sci. 6 (2013) 2196–2202.
[28] M. Hu, J. Chen, Z.Y. Li, L. Au, G.V. Hartland, X. Li, M. Marquez, Y. Xia, Gold nanostructures: engineering their plasmonic properties for biomedical applications, Chem. Soc. Rev. 35 (2006) 1084–1094.
[29] X. Yang, M. Yang, B. Pang, M. Vara, Y. Xia, Gold nanomaterials at work in biomedicine, Chem. Rev. 115 (2015) 10410–10488.
[30] S.E. Skrabalak, J. Chen, Y. Sun, X. Lu, L. Au, C.M. Cobley, Y. Xia, Gold nanocages: synthesis, properties, and applications, Acc. Chem. Res. 41 (2008) 1587–1595.
[31] J. Chen, C. Glaus, R. Laforest, Q. Zhang, M. Yang, M. Gidding, M.J. Welch, Y. Xia, Gold nanocages as photothermal transducers for cancer treatment, Small 6 (2010) 811–817.
[32] M.S. Yavuz, Y. Cheng, J. Chen, C.M. Cobley, Q. Zhang, M. Rycenga, J. Xie, C. Kim, K.H. Song, A.G. Schwartz, et al., Gold nanocages covered by smart polymers for controlled release with near-infrared light, Nat. Mater. 8 (2009) 935–939.
[33] M.S. Zielinski, J.W. Choi, T. La Grange, M. Modestino, S.M. Hashemi, Y. Pu, S. Birkhold, J.A. Hubbell, D. Psaltis, Hollow mesoporous plasmonic nanoshells for enhanced solar vapor generation, Nano Lett. 16 (2016) 2159–2167.
[34] J. Li, M. Yang, X. Sun, X. Yang, J. Xue, C. Zhu, H. Liu, Y. Xia, Micropatterning of the ferroelectric phase in a poly(vinylidene difluoride) film by plasmonic heating with gold nanocages, Angew. Chem. Int. Ed. Engl. 128 (2016) 14032–14036.
[35] H. Sawai, T. Mimitsuka, S.I. Minegishi, M. Henmi, K. Yamada, S. Shimizu, T. Yonehara, A novel membrane-integrated fermentation reactor system: application to pyruvic acid production in continuous culture by Torulopsis glabrata, Bioproc. Biosyst. Eng. 34 (2011) 721–725.
[36] W. Zhang, Z. Shi, F. Zhang, X. Liu, J. Jin, L. Jiang, Superhydrophobic and superoleophilic PVDF membranes for effective separation of water-in-oil emulsions with high flux, Adv. Mater. 25 (2013) 2071–2076.
[37] A.E. Kabeel, S.A. El-Agouz, Review of researches and developments on solar stills, Desalination 276 (2011) 1–12.
[38] O. Neumann, A.S. Urban, J. Day, S. Lal, P. Nordlander, N.J. Halas, Solar vapor generation enabled by nanoparticles, ACS Nano 7 (2012) 42–49.
[39] M.A. Shannon, P.W. Bohn, M. Elimelech, J.G. Georgiadis, B.J. Marinas, A.M. Mayes, Science and technology for water purification in the coming decades, Nature 452 (2008) 301–310.
[40] M. Elimelech, W.A. Phillip, The future of seawater desalination: energy, technology, and the environment, Science 333 (2011) 712–717.
[41] C. Chen, Y. Li, J. Song, Z. Yang, Y. Kuang, E. Hitz, C. Jia, A. Gong, F. Jiang, J.Y. Zhu, et al., Highly flexible and efficient solar steam generation device, Adv. Mater. 29 (2017) 1701756.
[42] M. Ye, J. Jia, Z. Wu, C. Qian, R. Chen, P.G. O'Brien, W. Sun, Y. Dong, G.A. Ozin, Synthesis of black TiOx nanoparticles by Mg reduction of TiO_2 nanocrystals and their application for solar water evaporation, Adv. Energy Mater. 7 (2017) 1601811.